Asymmetrically heated multi-stage travelling-wave thermoacoustic electricity generator

Wigdan Kisha[1*,2], Paul Riley[3], Jon McKechnie[1], David Hann[1]

[1]Faculty of Engineering. University of Nottingham, UK

[2]Faculty of Engineering. University of Khartoum, Sudan

[3]School of Mathematics, Computer Science & Engineering. City, University of London, UK

*Corresponding author. Email address: wigdan.kisha1@nottingham.ac.uk

Highlights

- A double-core travelling-wave thermoacoustic engine was modelled and tested.
- A novel operational methodology was proposed for heat addition into the two cores
- Using lower heat input in the first core increased the power output by 39%.
- Validation of DeltaEC models is done by comparisons with experiments.

Abstract

Recent developments of thermoacoustic engines have demonstrated that thermoacoustic technology is a viable option for waste heat recovery and low-cost electricity generation, Thermoacoustic technology is capable of converting low-grade heat to electrical power with only one moving part. Great reliance has been placed on evenly heated cores of multistage thermoacoustic engines, whatever the acoustic impedance is within the engine's core. This article proves that the unbalanced acoustic impedance within the cores can be effectively matched by using the asymmetric heat method. Accordingly, the thermoacoustic efficiency can be increased. DeltaEC code was employed to perform the numerical calculations and laboratory measurements were then taken to confirm the concept and validate the numerical model. Both numerical and experimental data show an increase in loop acoustic power with this new technique. DeltaEC simulation predicted an increase in the electrical power output from 24.4 W to 31.4 W, when heat supplied into the system went from (50%:50%) to a 40%:60% ratio, which matched an increase from 16.5 to 23 W in the experiments with no other change in the design except asymmetric heat input. DeltaEC results have implied that there is an optimal ratio of 30%:70%. It was also seen in the DeltaEC that the overall onset temperature decreased by about 40ºC for larger asymmetrical ratios of heat input, which is advantageous for this application.

Keywords: Regenerator, thermoacoustic, acoustic power, loudspeaker as a generator, DeltaEC

Nomenclature

A	Cross-sectional area of the feedback pipe, m²
A_g	Cross-sectional area of the regenerator, m²
a	Speed of sound, m/s
f	Working frequency, Hz
n	Impedance enhancement ratio
$P_{Ac.}$	Acoustic power, W
p_1	Pressure amplitude of oscillation, Pa
p_m	Mean pressure, Pa
Q_T	Total heating power, W
T_C	Cold temperature, K
T_H	Hot temperature, K
T_m	Mean temperature, K
U_1	Volumetric velocity, m³/s
u_1	Velocity, m/s
ω	Angular velocity, rad/s
X	Coordinate along sound-propagation direction, m
Z_1	Acoustic impedance, Pa/s.m^3
γ	Ratio of specific heat
Δ	Difference
ρ_m	Mean density, kg/m³
$\emptyset$	Phase difference, rad
Im[ ]	Imaginary part of a complex number
Re[ ]	Real part of a complex number
$*$	Complex conjugate
$\vert\ \vert$	Magnitude of a complex number

Abbreviations

AHX	Ambient heat exchanger
HHX	Hot heat exchanger
LA	Linear alternator
RPN	Reverse Polish notation
SAHX	Secondary ambient heat exchanger
TAE	Thermoacoustic engine
TBT	Thermal buffer tube
PID	Proportional-Integral-Derivative
PSWR	Pressure standing-wave ratio

1. Introduction

Affordable energy, in particular electricity [1] has the potential to improve the lives [2] of around one billion people that still have no access. The majority of these people either do not have mains electricity or it is too expensive for them [3]. Moreover, cooking activity requires particular attention in rural communities. A social assessment revealed that a smoke-free cooking stove that generates electricity is more attractive in rural and poor communities [4]. Various techniques that use low-temperature waste heat and renewable energy sources to generate electricity have the potential to address energy poverty levels [3] whilst at the same time minimise greenhouse gas emissions [1] and decrease fossil fuel consumption. These low temperature techniques can be categorised into Organic Rankine cycles, thermo-electric, Ericsson cycle, externally fired gas turbine, and Stirling cycles (piston driven and thermo-acoustic). A previous research has assessed the suitability of each technology for domestic electricity generation against key enablers to uptake in the rural communities, capital cost [5] and the requirements of local communities [6].

1.1 Organic Rankine Engines (ORE)

Ramos et al [7] propose solar driven ORE for generating electricity in the built environment and Kiyarash presented a review of ORE for small scale applications [8] using a variety of waste heat sources. However, Li points out the environmental impact of the various working fluids [9] making it questionable if OREs are suitable for domestic use in rural areas. The complexity and cost of ORE is a further inhibitor to uptake.

1.2 Thermo-electric generators (TEG)

Various proposals for using TEG for generating electricity from waste heat for domestic use have been made, for example from the heat of a car exhaust [10]. However, Elghool [11] highlights that although the basic TEG cost is low, it requires considerable balance of plant, especially heat sinks that significantly increase the costs to the end-user. Electrical power from TEG is a function of the square of the hot to cold junction temperature [12] and ambient temperatures are relatively high in the target countries. Reducing the size of heat exchangers to save cost results in a disproportionally large loss in electrical output. When combined with the present relatively low efficiency of TEGs [13] and the theoretical loss when powered from a flame source [14], may explain their lack of uptake except in a few low volume cases [15].

1.3 Ericsson Cycle

It was named after an inventor John Ericsson who designed the cycle in 1833. The compression and expansion of the gas parcels occur in a counter-flow heat exchanger isolated from the hot and cold heat exchangers [16], with a number of valves separating the different parts. One of the significant drawbacks of the cycle is its valve mechanism, which increases the cycle's complexity, and manufacturing cost, and therefore, it minimises the reliability.

1.4 Externally fired gas turbine (EFGT)

The externally fired gas turbine (EFGT) is a novel technology that utilises waste heat from the turbine in a recuperative process [17]. The EFGT is being developed for small and medium-scale power and heat generation. One of the most important challenges is the requirement of using a high temperature heat exchanger to transfer the combustion gases into the working gas. The availability of high-temperature material, effective welding and sealing would be problematic, and therefore, results in a high manufacturing cost.

1.5 Stirling Cycle

1.5.1 Piston Stirling Engines

Invented in 1816, by Dr Robert Stirling, the cycle takes heat from a hot source to a cold one to extract energy. This energy can be converted to electricity [18] in various ways. A gamma type of Stirling piston engine for waste heat recovery was proposed by Wan et al [19] and Yoshihara compares other Stirling engine formats, including the free-piston engine that removes the crankshaft to reduce cost [20].

1.5.2 Thermo-acoustic Engines

Removing components is a method for reducing cost over and above the Yoshihara's proposals, leads to the travelling wave Thermo-Acoustic Engine (TAE) which works on the Stirling cycle but with no moving parts. In 1969 Rott investigated thermal instability in tubes[21] and Ceperley proposed a travelling wave thermo-acoustic engine [22]. Swift developed a theoretical framework for designing thermo-acoustics engines [23] leading to a 13.8 bar helium engine that delivered 630 W of electrical power [24]. As with Piston base Stirling engines TAE have various configurations, the main categories being standing wavs and travelling wave [25]. Standing-wave engines have been investigated intensively [24]. They are not efficient because of the inherent irreversible thermoacoustic conversion processes [26], although recent work using a two-stage standing-wave configuration has achieved over 30W with low heat input [27]. Travelling-wave TAEs employ a compact acoustic network to obtain the proper time phasing within the regenerator so that the gas undergoes a Stirling-like thermodynamic cycle to deliver acoustic power from heat energy [28] and they are therefore more efficient. Significant progress on the efficiency of TAEs has been achieved over the last 10 years mainly using travelling wave engines.

An early version of the travelling-wave TAE, the well-known torus configuration travelling-wave engine developed by Backhaus and Swift, delivered 710 W acoustic power. It also achieved a respectable thermal to acoustic efficiency of 13%, and a relative Carnot efficiency of 30%. This configuration used 30 bar pressurised helium as the working gas at a high operating temperature of 725˚C [29], and thus it would not be useful for developing world applications. Up to now, the most efficient traveling-wave TAE has achieved a efficiency of 49% of Carnot efficiency [30].

Travelling-wave TAEs with a single-core design are typically more efficient for high temperature operation and have a higher onset temperature [31] There have been attractions in using single-stage TAEs for developing world applications [32] due to their lesser complexity [33], However, research has led to the use of multiple thermoacoustic cores in the thermoacoustic travelling-wave engine to enable the onset of oscillation at a much lower temperature [31] and also to enhance the thermoacoustic amplification [34].

The most advanced and powerful of these multistage systems contain two [35] three [36] or four [37] cores, generating 204 W, 1.57 kW,(against a target of 3 kW) and 1.2 kW of power, respectively and Aster, a Dutch company are designing a 4 stage 10 kW unit using a turbo alternator. [38] This level of power was achieved by pressurising the gas to as much as 6 MPa. Pressurisation of the working gas can increase the power output by the order of the square root of the pressure. However, these mainly use high pressure helium as the working fluid that present sealing and cost problems and make them unsuitable for domestic power applications, although the increased power may be suitable for village wide use.

Thermoacoustic engines can be integrated into efficient wood cooking stoves to provide electricity while cooking [39], but the output and efficiency have to date proven to be too low [32]. Recent social science studies have suggested that an ideal system would generate about 100 W of electrical energy and cost less than $100, and even 20 W conveys considerable benefits [40]. If research can increase the power output, the system could benefit the 3.3 billion who live in rural areas, of whom almost half use biomass for cooking but have no access to electricity [41]. There is a reluctance to take up efficient "smokeless" stoves and studies have shown that this reluctance can be overcome if the stove can also generate enough electrical power for small appliances such as LED lights (< 5 W), charging mobile phone (5 W), radio (< 1 W), or an iPad (10 W) or small laptop (< 40 W) [1,6] . This improvement could result in an increase in the uptake of "smokeless" stoves and would have a secondary benefit, since smoke-related diseases are the second-biggest killer in the developing world after malaria [42].

To meet this requirement, a system must be simple to construct and cheap to maintain. An assessment of technologies carried out in 2014 [5] identified that thermoacoustics integrated into a stove could be more cost-effective than most other electrical generation technologies (when efficiencies increase) except hydroelectricity, although the decreasing cost and increasing efficiency of solar power in recent years have brought the latter back into contention [43], although [44] suggests that there is still research needed to enhance the stability and manufacturability of this solar power technology.

The thermoacoustic engine (TAE) is a new and promising technology that utilises heat to produce high-intensity sound waves that, in turn, can be utilised to generate electricity or refrigeration. There are many applications for thermoacoustic technology, such as refrigeration to obtain low cooling capacity [45] as well as high cooling capacity [46] electricity generation for both waste heat recovery [15,16] and high temperature applications [17,18] monitoring of nuclear fusion temperatures [47,48]. A TAE is highly reliable and is easy to construct since there are no mechanical moving parts except the alternator, which makes it ideal for application in the developing world. The TAE consists of an acoustic resonating tube and a core that is composed of a section of porous media between a hot and a cold heat exchanger [49] The expansion and contraction of the air between these heat exchangers causes pressure fluctuations. These pressure fluctuations propagate around the loop to return to the heat exchangers. If the pressure fluctuations return in phase, a strong acoustic field can be generated. An alternator, such as a loudspeaker, is used to harvest these oscillations to produce electrical current.

Once the thermal gradient has generated the acoustic power, electrical power can be harvested using the only moving part, the acoustic to electrical transducer. This transducer may be a linear alternator [50] or a rotating device [51]. The introduction of the acoustoelectric transducer alters the acoustic impedance within the system, and therefore, degrades efficiency. The proper acoustic impedance conditions can be obtained by optimising the regenerator dimensions and/or position [52] or by adding impedance matching techniques such as a stub branch [53] compliance resistance tube [54] variable electric load resistance [55] ultra-compliant loudspeaker [56].

To meet this need, the SCORE (**S**tove for **Co**oking **R**efrigeration and **E**lectricity supply) consortium (www.score.uk.com) was created in 2007. It was managed by the University of Nottingham and worked with Practical Action to address this problem by developing clean, efficient cooking stoves that generate electricity. The social research carried by SCORE revealed that the electrical power rating of an ideal power generating stove in the developing world should target a range of electrical power output of 50 - 100 W, with a manufacturing cost that should ideally not exceed 200 pounds [1]. However, the different designs created for SCORE either the electrically heated prototypes [32,57] or the ones integrated to cooking stoves [58,59] and those of researchers around the world [27,55] has produced a range of variations all striving to reach the 50 – 100 W target to make the technology viable. In addition, there has been related research in the development of coolers and refrigerators based on thermoacoustic technology [45].

One of the developments from SCORE is a twin-core design thermoacoustic engine [58]. This system is not yet capable of meeting the target but has managed to generate 12.6 W when integrating to a wood burning stove [60]. In this design, the two cores were placed side by side so that the hot gases from the fire heated them evenly. This paper explains and proves that the electrical power output from this twin-core system can be increased significantly by heating each core by different amounts depending on the location in the feedback tube. Evenly heated core has led to asymmetric impedance within the two symmetric engine cores. A novel asymmetric heat methodology has applied to the two hot heat exchangers, and this has significantly balanced the acoustic conditions throughout the system. Up until now, no previous study has reported the effectiveness of the asymmetric heat distribution in improving the thermoacoustic effect within the thermoacoustic cores of multistage thermoacoustic systems.

2. Theoretical Modelling

2.1 DeltaEC software

For an in-depth understanding of the behaviour of the thermoacoustic system considered in this research and to predict the performance of the existing prototype, a design software code referred to as DeltaEC (**D**esign **e**nvironment for **l**ow-amplitude **t**hermo**a**coustic **E**nergy **C**onversion) was chosen. DeltaEC is a specialised software that has emerged as a powerful tool for analysing TAEs and refrigerators [49]. DeltaEC is a python-based numerical code written by Swift and Ward from Los Alamos National Laboratories group, and it is based on the linear thermoacoustic theory. DeltaEC numerically integrates the continuity, momentum, and energy equations to obtain the pressure, volumetric velocity and the phase difference between them along the thermoacoustic devices. DeltaEC enables users to construct the geometry of the system from segments previously defined in the software, such as ducts, heat exchangers and regenerators. It numerically integrates the wave equation and other equations, such as the energy equation, throughout the whole system in one spatial dimension based on a low-amplitude “acoustic” approximation and sinusoidal time dependence of the variables [61]. DeltaEC adopts a shooting method to satisfy various boundary conditions set by the user. The governing equations used in DeltaEC are shown in [62].

2.2 Description of the model of the current system

Since this research targets the developing world, atmospheric air is selected as the working gas. The maximum high and low temperatures were chosen to match experimental values of between 90ºC and 650ºC, respectively. The total heating power was added into the system via two identical electrical heaters and it was varied in the range of 2.1 - 3 kW. This mimics the input of the heat from combustion. The total heat was split by different percentages between the two stages. The predictions obtained by the DeltaEC simulation have shown that changing the heat ratio for each hot heat exchanger (HHX) could affect the performance. Accordingly, the heat ratios were set as 40%:60%, 50%:50%, 55%:45%, and 60%:40% to match those in the experiments. The system operates at 73 Hz working frequency. To verify the numerical results against the lab data, the load resistance of the loudspeaker was set to 35.5 Ohm. The DeltaEC model was verified against the experimental data shown below to confirm the findings.

The model have been validated against the simulation without varying the heat input ratio. This section to show the behaviour of the model. The functional diagram of the model used in the DeltaEC simulation is presented in Fig. **1(b)**. The model was constructed using several DeltaEC segments such as DUCT, HX, STKSCREEN, STKDUCT, BRANCH, and IESPEAKER with the same design parameters of the existing prototype, as displayed in Fig. **2**. The required input parameters for each segment are explained in detail in [61]. The starting point of the simulation is at $x = 0$, which is shown in Fig. **1(b)** at the cold end of the main AHX of engine 2. The acoustic wave travels anticlockwise until it returns to $x = 0$. At this point, the target boundary conditions of the model are matched to the starting conditions. The

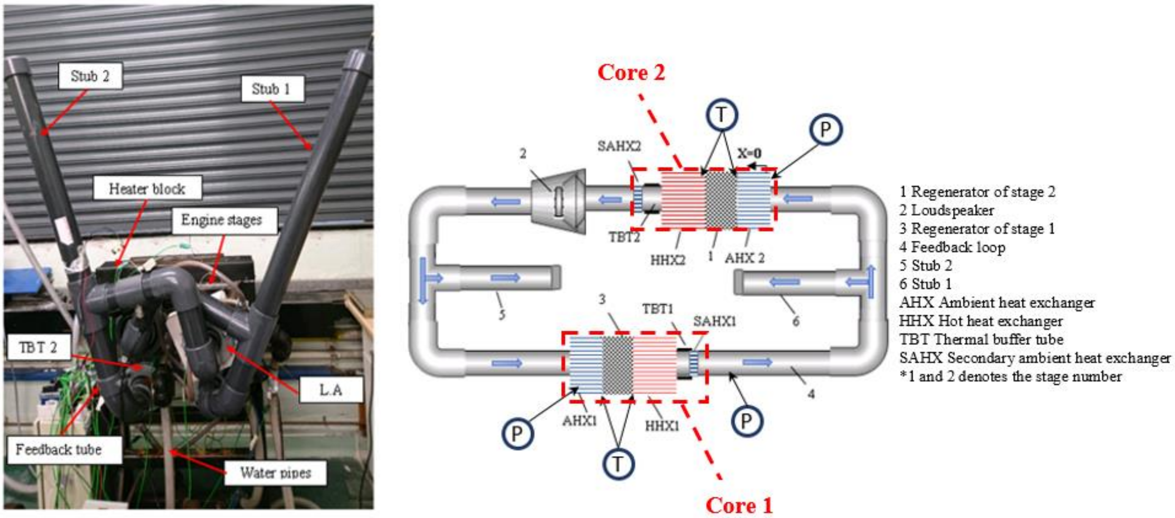

Fig. 1: The two-stage looped-tube thermoacoustic electricity generator. **(a)** Photo of the apparatus. **(b)** Schematic diagram provided with a key to show the system components and the location of the measurements: P for pressure readings, and T for temperature.

matching conditions are the pressure amplitude, the volumetric velocity amplitude, and their phases. The blue arrows in the schematic in Fig. **1(b)** indicate the dominant flow of the travelling wave through the system.The steps involved in DeltaEC simulation of the asymmetrically heat thermoacoustic electricity generator are outlined in Fig. **3**.

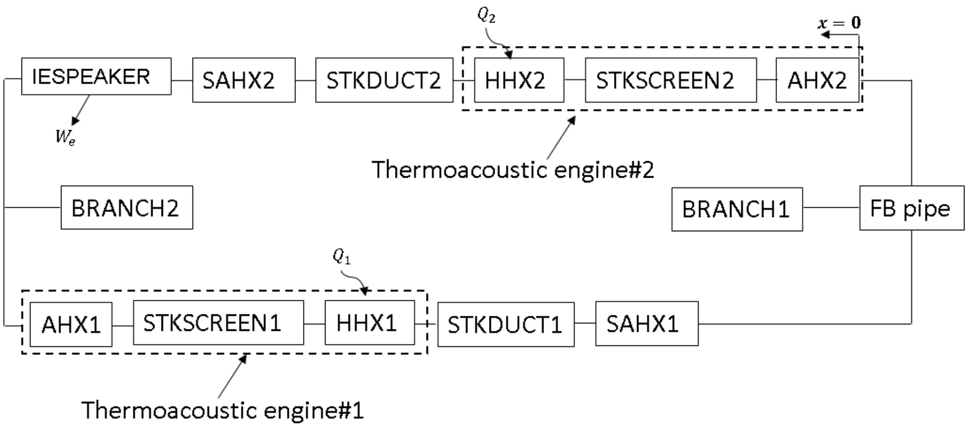

Fig. 2: DeltaEC segments block diagram for the two-stage looped-tube thermoacoustic electricity generator showing the system components, and the distribution of the heat in the two cores, Q_1, and Q_2, respectively.

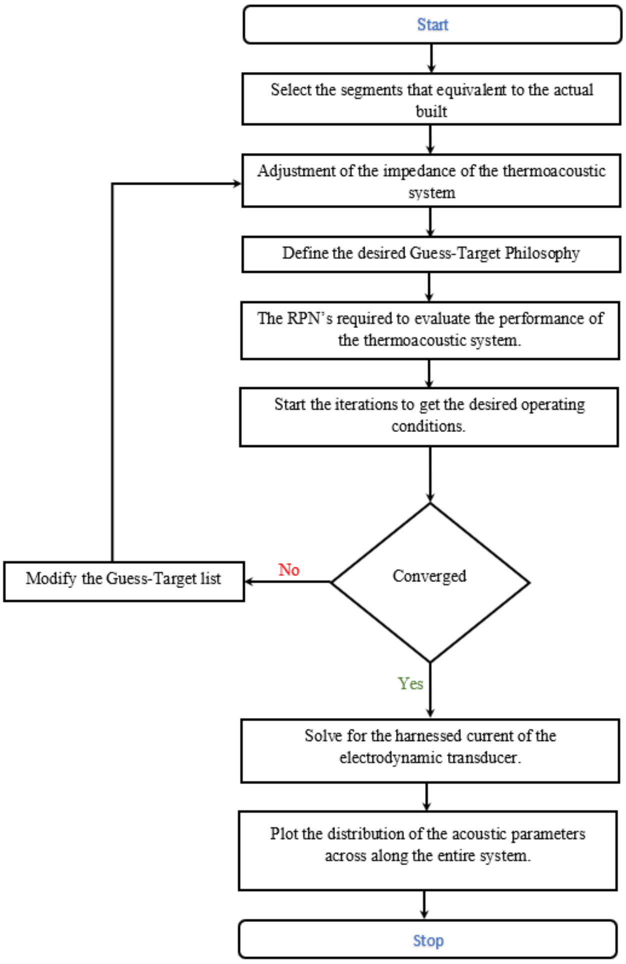

Fig. 3: Flow chart of the DeltaEC iteration process of the asymmetrically heated thermoacoustic engine. This process can be applied to any looped tube thermoacoustic system with a power extractor.

3. Experimental Methods

To validate the model a series of experiments were undertaken in the SCORE engine. The SCORE engine comprises a two-stage thermoacoustic engine designed to operate in travelling-wave mode. The system uses a loudspeaker that works in reverse as linear alternator, although there are other alternatives such as bi-directional turbines that are clearly summarised in [63] For this application, the driving force was the cost and availability of the parts in remote villages. Two matching stub branches were used to correct the acoustic filed, as illustrated in Fig. **1**.

The engine is essentially a looped-tube configuration, The looped-tube arrangement offers the advantage of utilising a low-temperature heat source with a lower temperature gradient through each stage either two [31] or more [64]. The general arrangement of each engine (core) consists of a regenerator that is located between two heat exchangers: an ambient heat exchanger (AHX) and a hot heat exchanger (HHX). The core also contains a thermal buffer tube (TBT) and a secondary ambient heat exchanger (SAHX), as shown in Fig. **1(b)**.

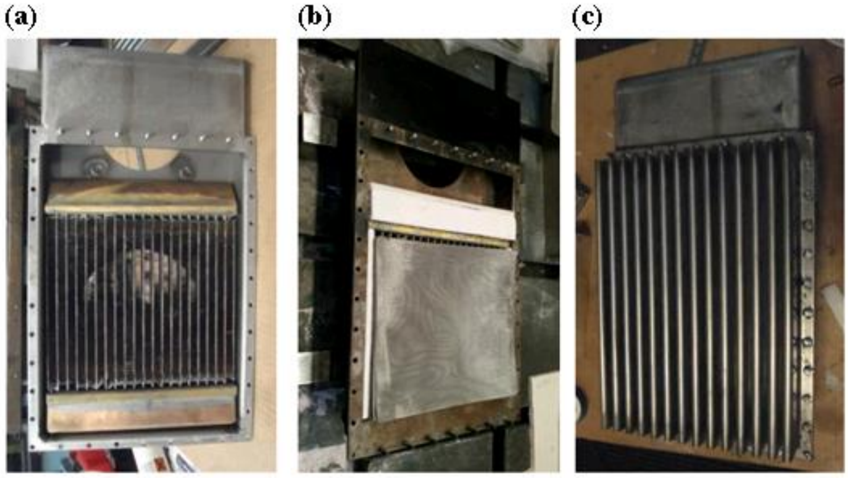

Fig. 4: Photos of the components used to build the two cores of the thermoacoustic electricity generator. **(a)** The ambient heat exchanger. **(b)** The regenerator. **(c)** The convoluted plate hot heat exchanger.

The AHX Fig. 4**(a)** is made of the core of a commercially available low-cost car radiator, suitably modified to fit the TAE. It has a rectangular cross-section of $25 \times 21.7\ cm$, with tube plates of $1\ cm$ pitch and $1\ mm$ spaced fins. AHX is cooled by tap water, which means no pump is required for this system. The HHX Fig. **4(c)** is made of $3\ mm$ thick convoluted stainless steel plate ($23.3 \times\ 30.7\ cm$) to achieve a quick warming-up time, and also to maintain a low cost for the engine core. To provide a controlled and repeatable input of heat energy, the HHX is heated by two external custom-made electrical heaters. Each heater consists of 12 nichrome heating coils connected in series, and all are embedded inside two individual enclosure heating blocks. To control the temperature of the two heaters, the system is equipped with two separated PID (Proportional-Integral-Derivative) controllers. The HHX plate is welded to a flange that is designed to be directly bolted to the engine housing and provide a good seal. The regenerator Fig. **4(b)** is the key component where the thermoacoustic effect takes place. The interaction between the air and the wall of the regenerator forces the gas parcels to undergo a Stirling-like cycle, and therefore producing acoustic power. It is sandwiched between the AHX and HHX and is formed by stacking 50 pieces – 80 mesh stainless-steel screens machined to a required size of $20\ \times\ 20\ mm$. The mesh wire has a diameter of $95\ \mu m$ and a pitch of $250\ \mu m$. The dimensions of all parts of the system are given in detail in Table **1**.

Table 1. Design parameters of the components of the double-core thermoacoustic system

Part	Parameter	Value
	Length, L (mm)	25
Ambient heat exchanger	Porosity, $\emptyset$ (%)	70
	Plate spacing, $2y_0$ (mm)	2.934
	Length, L (mm)	12
Regenerator	Porosity, $\emptyset$ (%)	73
	Hydraulic radius, r_h (μm)	97
	Length, L (mm)	40
Hot heat exchanger	Porosity, $\emptyset$ (%)	75
	Plate spacing, $2y_0$ (mm)	9
Thermal buffer tube	Area, A (m^2)	8.33E-03
	Length, L (mm)	10
Secondary ambient heat exchanger	Porosity, $\emptyset$ (%)	71.3
	Plate spacing, $2y_0$ (mm)	2.934
Tuning stub	Area, A (m^2)	3.85E-03
	Length, L_{stub} (m)	0.70
Feedback loop	Area, A (m^2)	3.85E-03

The AHX, regenerator, and HHX all are positioned between the upper and lower housings. The upper housing is 3 mm thick and was manufactured from mild steel as it does not directly experience high temperatures. In contrast, the lower housing is in direct contact with the HHX. It is therefore made of 3 mm-thick stainless steel, which has a low thermal conductivity, so the parasitic heat losses are minimised. To separate the SAHE from the hot gases and reduce heat dissipations, a section of stainless-steel pipe (the TBT) is positioned immediately below the HHX. An SAHX is placed after the TBT to cool the air, so it doesn't pass to the alternator (loudspeaker). As shown in Fig. **1(b)**, the two engine stages are connected using two lengths of 70 mm inner diameter PVC pipes called a feedback loop in a $\frac{\lambda}{4}/\frac{3\lambda}{4}$ ratio. There are two additional 70 mm diameter PVC pipes perpendicular to the feedback loop named tuning stubs. The function of the stub branches is to enhance the impedance matching between the acoustic wave and the LA, and to maintain the required phase angle between the velocity and pressure in a travelling-wave condition through the regenerators. All the pipework and the fittings are PVC to reduce the cost of the system, as affordability is a key factor.

The system is coupled with a single loudspeaker (model JL 6W3v3-4) to harvest the electrical power. Basically, the acoustic power generated from the two engine stages flows into the loudspeaker and oscillates its diaphragm, and thus moving a coil in a magnetic field that generates voltage. The loudspeaker is connected in series after the SAHX of the second engine to ensure better cooling of the air. Using only one loudspeaker has led to a lower cost and a simple design. This configuration aids suppression of the acoustic streaming which might cause non-linear heat dissipations from an HHX. The specifications and the Thiele/Small parameters of the loudspeaker are presented in Table **2**.

Table 2. Thiele/Small parameters of the loudspeaker used in the double-core system to harvest the electrical power

Area, $A_{L.A}$ (m^2)	**Force factor, Bl $(T.m)$**	**Electrical resistance, R_e (Ω)**	**Electrical inductance, L (mH)**	**Moving mass, M (g)**	**Stiffness, K (N/m)**	**Mechanical resistance, R_m $(N.s/m)$**
1.96E-02	14	4	10	20	4778	0.18

Temperatures were monitored using eight thermocouples (Type-K RS Components, ±1ºC accuracy) embedded at various locations. Six of them were in the thermodynamic section to measure the hot and cold temperatures of each regenerator, and the rest were used to measure the cooling water flowing into and out of the AHX. A water flow meter (Type TM-47X, FMS Rotameter RSeries 2000, ±1.2% accuracy of indicated flow) was employed for monitoring the water flow rate of the system. Three absolute pressure transducers (model IMPRESS: IMPA5000-1A4-BXV-00-063, ±0.1% accuracy) were inserted at important locations to capture the pressure variation. Two of them were attached to each AHX, and one was connected to the feedback loop. One differential pressure sensor (model ABPMJJT015PGAA5, ±0.25% accuracy) was installed in the loop to capture the volumetric flow rate, and therefore to estimate the acoustic power of the loop. The readings of the thermocouples and the pressure transducers were recorded through a cDAQ Data Acquisition system connected to a custom-built LabVIEW Program. A wide-range power variable resistor (model VISHAY®, range 0-100W, and ±0.1% accuracy) was adopted as an electrical load for the loudspeaker in order to harvest the electric power from the system. This was set to 35.5 Ohms to match the model. The voltage difference and the current output from the loudspeaker were measured by a power analyser (model KinetiQ PPA2530, ±0.04% accuracy).

In order to quantify the performance of the system, it is important to determine the heating power, the acoustic power and the electric power output. The most complicated parameter to measure is the acoustic power, which is defined as a time-average energy flux accompanied by pressure oscillations and velocity of the working gas. Accordingly, measurements of the pressure amplitude, volumetric velocity amplitude, and their phases are mandatory for estimating the loop acoustic power.

One of the best-known tools for assessing acoustic power is the so-called two-pressure sensor method [65]. Conceptually, this method employs two absolute pressure sensors placed adjacent to each other to obtain the velocity of the oscillating gas. Perhaps the most serious uncertainty of this method is the accuracy of the phase angle between the pressure and the velocity. To reduce error in the acoustic power, the two transducers should be separated by a velocity antinode and a relatively large distance of the order of 60 cm. The accuracy of the measuring sensor for the phase angle measurement should be less than 0.01 degrees. Hence, a more durable way of measuring the acoustic power can be achieved using an alternative method referred to as "gradient method" [66], which is employed in the current system. The method utilises one differential pressure sensor plus one absolute pressure transducer based on the acoustic pressure gradient in the working gas to directly calculate the mass of the air between the two sensors, the acoustic velocity, and the acceleration. The distance between the two sensors is small compared to the two-microphone method, so no empirical correction for acoustic loss is required. Acoustic power propagation in the feedback loop is defined as:

$$P_{Ac.} = \frac{1}{2}\mathrm{A}.\,Re(p_1 u^*{}_1) \tag{1}$$

$$= \frac{1}{2}\mathrm{A}.\,\hat{p}_1 \hat{u}_1 \cos \emptyset \tag{2}$$

Here: A is the cross-sectional area of the feedback loop (m²), p_1 is the pressure amplitude of oscillation (Pa), which is the signal obtained from the absolute sensor, and u_1 is the acoustic velocity (m/s) and can be given as:

$$u_1 = \frac{\Delta p_1}{\omega \rho_m \Delta x}(-\,\mathrm{i}\cos \emptyset + \sin \emptyset) \tag{3}$$

Where: Δp_a is the output signal from the differential pressure sensor (Pa), Δx is the distance separates the two probes of the differential sensor (m), $\emptyset$ is the measured phase between p_1 and Δp_1, ω is the angular velocity (rad/s), and ρ_m is the mean density (kg/m³).

Subsequently, the acoustic power can be found by substituting the real part of the acoustic velocity in Eq.(2):

$$P_{Ac.} = \mathrm{A}.\,\hat{p}_1 \frac{\Delta \mathrm{p}_1}{2\omega \rho_m \Delta x} \sin \emptyset \tag{4}$$

4. Results and discussion

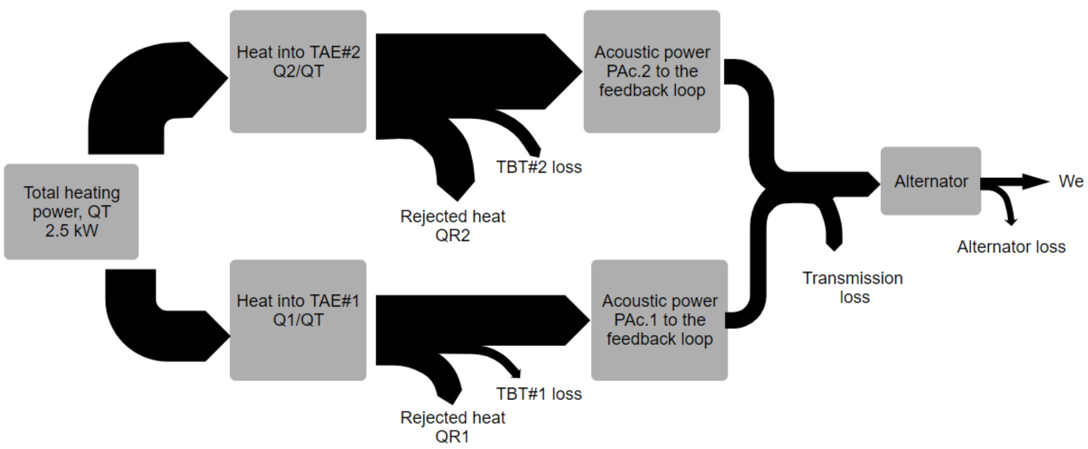

Fig. 5: Sankey diagram visualising the energy distribution in the thermoacoustic system.

The heat flow of the system is summarised and illustrated in Fig. **5**. The net heating power is used to power the two thermoacoustic engines TAE1 and TAE2, where most of this heat is converted into acoustic power by the engines. The remaining heat of the thermoacoustic engines is removed away by the ambient heat exchangers and lost to the thermal buffer tubes. Acoustics power is then flowed into the alternator and lost due to transmission loss on the feedback pipe. The alternator is eventually extracted the electrical power from the net acoustic power.

Fig. **6** to **11** demonstrate the variation of the key acoustic parameters throughout the system obtained from the DeltaEC simulation. The four curves in each graph correspond to the various heat input ratios directed into the two HHXs: 40%, 50%, 55% and 60% of the heat was directed into HHX1, and the power in core 2 was set so that the total heat supply remained constant. No other variables were adjusted. The changes in the pressure amplitude of oscillation are displayed in Fig. **6**. It is obvious that all the curves have the same trend for all the heat supply percentages. The numbers shown in the graphs identify the locations from the schematic representation in Fig. **1(b)**.

The pressure amplitude drops at each of the two regenerators (1 and 3) because of their flow resistance. It also decreases across the loudspeaker (2) due to its acoustic resistance, which is the product of the mechanical resistance Rm, electrical resistance R_e, load resistance R_L, compliance C_{LA} and inertance L_{LA}. The two stubs do not influence the pressure amplitude significantly.

The pressure standing-wave ratio (PSWR) in the system is approximately 2.97 because of the reflections where the cross-sectional area of the resonator changes. For practical travelling-wave systems, a PSWR of less than 1.8 is considered good [67]; this can be achieved using several techniques such as varying the length of the branch pipe. There is a higher pressure drop through the alternator (loudspeaker) when 40% of the heat is directed to HHX1, which indicates better extraction of the electric power. In other words, a 48% increase in the electrical power output can be achieved when the balance of heat goes from 50% to 60% in the second engine. The location of the pressure anti-nodes altered slightly in the four heat supply ratios, particularly near the end of the feedback loop due to the small change in the operating frequency.

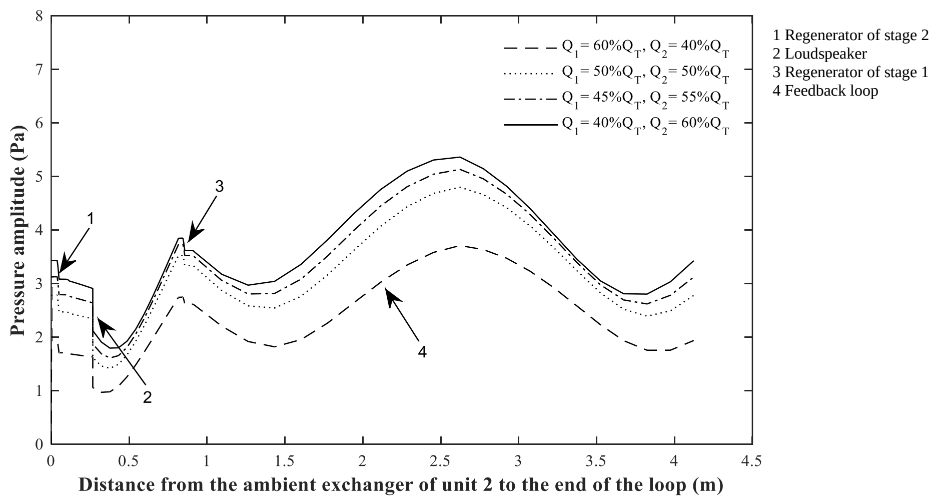

Fig. 6: Peak pressure variation along the loop for different heat input ratios: Q_1 in heater 1 and Q_2 in heater 2, and a fixed 2500W total heat input. Numbers are consistent with Fig. **1(b).**

The distribution of the acoustic volumetric velocity throughout the thermoacoustic loop for different ratios of the total heating power is shown in Fig. **7**. No obvious differences are observed in the trend of all the curves other than those noted previously. The volumetric velocity is low at the AHX of regenerator 1 and regenerator 2 (locations 1 and 3), which is the expected design to eliminate viscous dissipations and to enhance the amplification of the acoustic power in the system. The volumetric velocity is effectively reduced due to the enlarged cross-sectional area of the thermoacoustic core, which is crucial for powerful operation. Also, the curves show that volume flow rate has a second low value at location 6 (stub branch), which corresponds to the location of the highest pressure amplitude. Moreover, there is a high decrease in the volume velocity at this location, which indicates that the stub removes part of the volumetric flow from the loop. In contrast, there is a significant increase in the volume flow rate across the two regenerators as a result of the increasing temperature gradient. After the alternator (loudspeaker) and before the SAHX, there is a region between locations 1 and 5 where the pressure amplitude decreases and volumetric velocity increases. Of the four heating power ratios, the $Q_1 = (40\%Q_T)$: $Q_2 = (60\%Q_T)$ has the highest pressure amplitude and the highest volumetric velocity amplitude compared to the other ratios, while the $Q_1 = (60\%Q_T)$: $Q_2 = (40\%Q_T)$ produces the fewest oscillations.

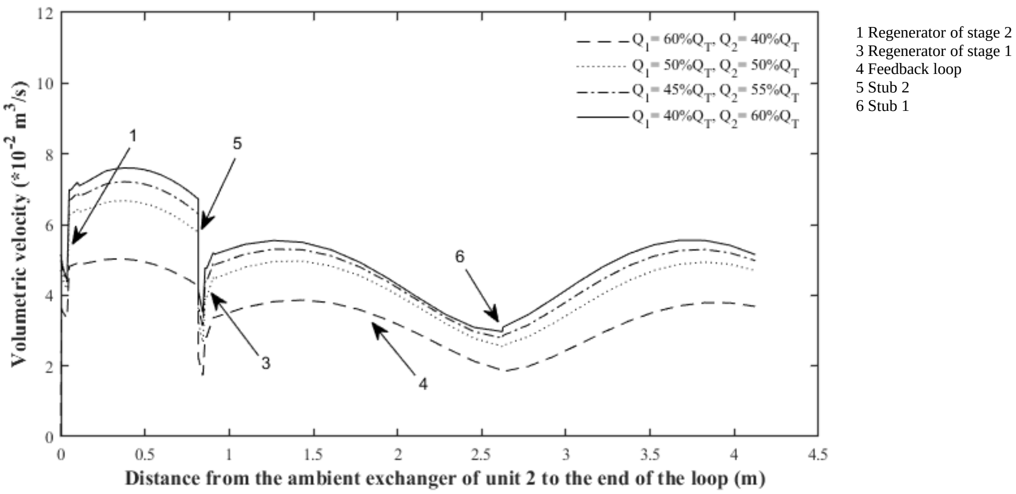

Fig. 7: Peak volumetric velocity variation along the loop for different ratios of the heating power: Q_1 in heater 1 and Q_2 in heater 2, and a fixed 2500W total heat input. Numbers are consistent with Fig. **1(b)**

The mean temperature distribution with respect to the axial coordinate is presented in Fig **8**. For the four tested heating power ratios, the temperature decreases along the thermal buffer tubes TBT2 and TBT1 from hot temperature to mean temperature. The length of the thermal buffer tube should be longer than the peak-to-peak displacement amplitude [49]. Too short thermal buffer means inadequate thermal insulation. On the other hand, too long thermal buffer tube means higher viscous loss. The mean temperature of the gas across the pipe work is independent of x for all the heat input ratios. The graph shows a hot end temperature of around 585 K in the second thermoacoustic engine, and in the order of 530 K in the first engine when 40% of the heating power is supplied to HHX1. For $Q_1 = (40\%Q_T)$: $Q_2 = (60\%Q_T)$ the hot end temperature is around 533 K in the second engine and 637 K in the first engine.

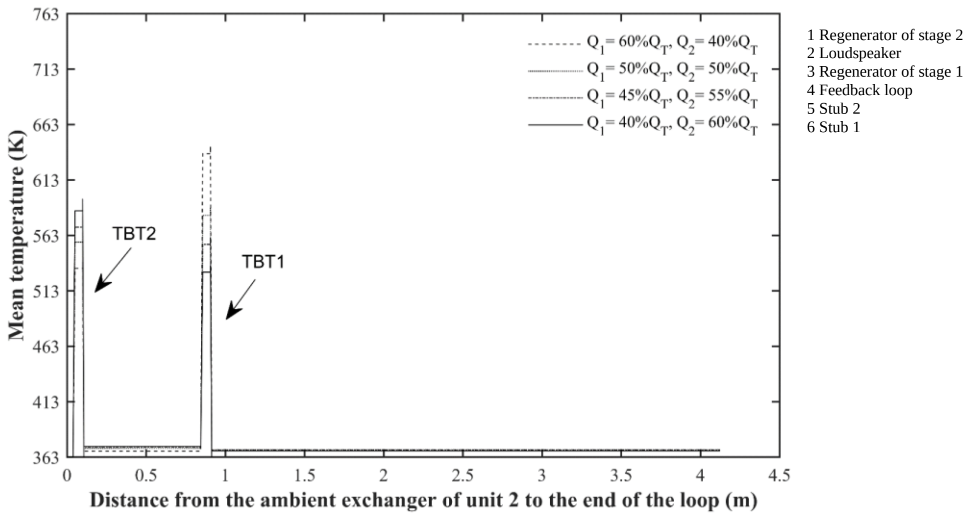

Fig. 8: The variation of the mean temperature of the working gas along the loop for different heat input percentages: Q_1 in heater 1 and Q_2 in heater 2, and a fixed 2500 W total heat input. Numbers are consistent with Fig. **1(b)**

The acoustic impedance is plotted in Fig. **9**. For all the heat ratios, there are two higher acoustic

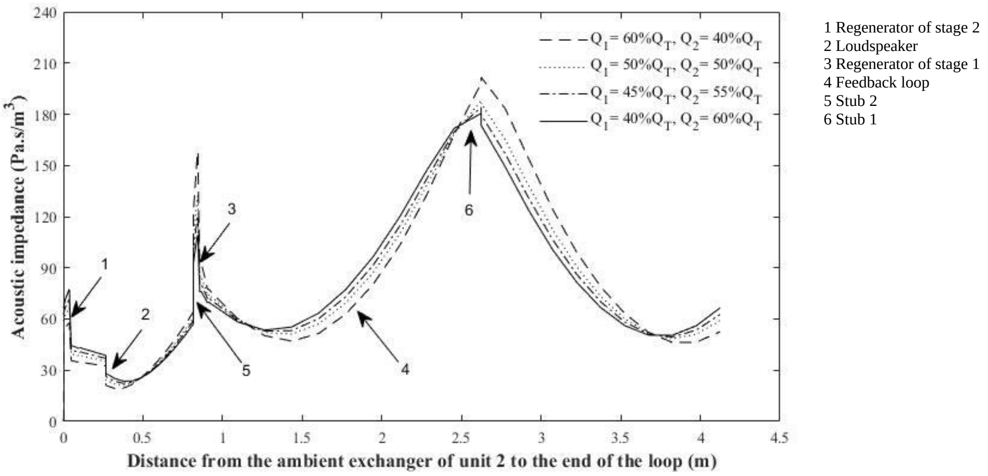

Fig. 9: Acoustic impedance variation along the loop for different heat input percentages: Q_1 in heater 1 and Q_2 in heater 2, and a fixed 2500 W total heat input. Numbers are consistent with Fig. **1(b)**

impedance values at locations 1 and 3 that correspond to the thermoacoustic regenerators. These values represent 14.4 and 7.2 times the specific acoustic impedance of the gas ${\rho_m a}/{A_g}$ when the heat is equally distributed between the two engines. These values change to 11.9 at regenerator 1 and 8.3 at regenerator 2 when applying 40%:60% in the two HHXs. This reflects that the impedance in the second core is relatively better when using two-thirds of the heat in the second stage. In travelling-wave TAEs, a standard practice is to set the absolute value of the regenerator impedance within the range of 10-20 times the specific acoustic impedance to limit the impact of viscous dissipations in the regenerator [31]. The acoustic impedance dropped at the alternator (location 5) where the volumetric velocity was constant at the two sides of the diaphragm. At the tuning stubs (locations 5 and 6), the impedance decreased due to the constant pressure amplitude at the junction between the stub and the feedback tube. To optimise the whole system, introducing the stubs within the loop reduced the reflections and compensated the acoustic impedance drop caused by the alternator (loudspeaker).

The phase angle between the pressure and the volumetric velocity of oscillation throughout the loop is illustrated in Fig. **10**. The graph again shares the same trend among the four different heat ratios being added to the two cores. For all the cases, the two regenerators (locations 1 and 3) are close to zero, which would be expected for a travelling wave. After the alternator (location 2), there is a rapid decrease in the phase angle. In contrast, there are two sharp increases in the phase at the two stubs (locations 5 and 6) to counteract the sharp decrease in the phase angle caused by the alternator (loudspeaker). When supplying 2.5 kW total heat power, Q_T , with different ratios across the two stages, the phase angle within the system is altered. For example, applying $60\%Q_T$ instead of $40\%Q_T$ into the HHX2 shifts the phase angle within the first regenerator from $-40°$ to $-18°$. The phase angle range within the feedback loop changes from $-40° < \emptyset < 40°$ to $-34° < \emptyset < 34°$. One of the design strategies to fulfil in travelling-wave TAEs is that the phase angle between the pressure amplitude and the volumetric velocity amplitude should be close to zero or slightly negative within the regenerator. In addition, near travelling-wave condition should be maintained in at least one part of the feedback tube. Thus, the amplification of the acoustic power within the regenerators can be maximised and the acoustic power dissipation within the feedback pipe can be minimised. The phase angle at 2.7 m equals zero when using 60% in HHX2, so using one-third

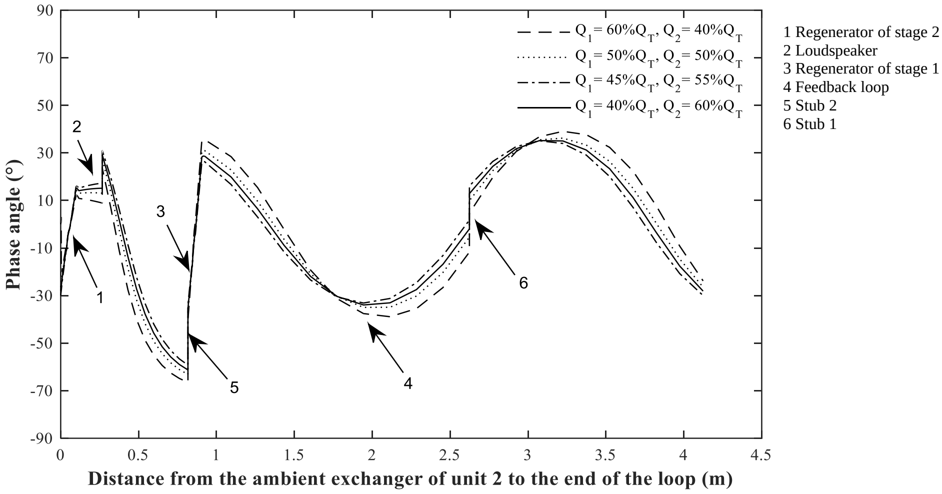

Fig. 10: Distributions of the phase difference between the pressure wave and the volumetric velocity for different heat input ratios: Q_1 in heater 1 and Q_2 in heater 2, and a fixed 2500 W total heat input. Numbers are consistent with Fig. **1(b)**

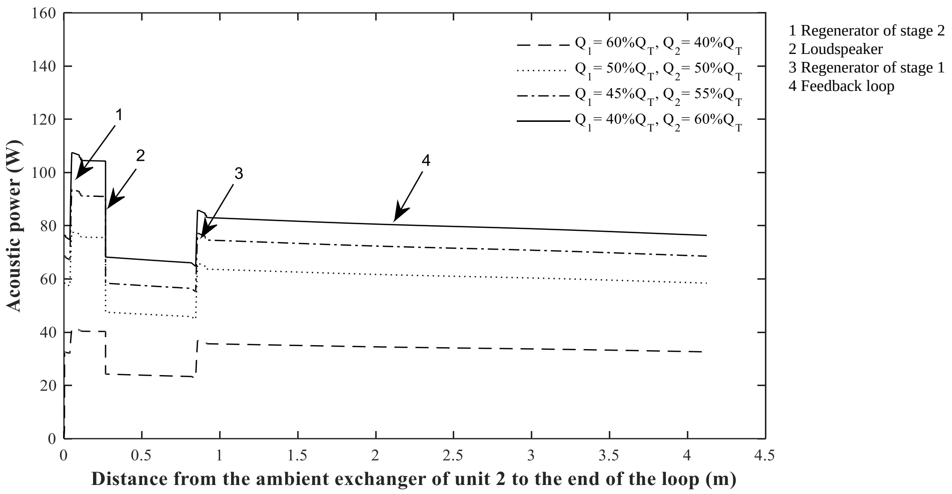

Fig. 11: Acoustic power variation along the loop for different heat percentages: Q_1 in heater 1 and Q_2 in heater 2, and a fixed 2500 W total heat input. Numbers are consistent with Fig. **1(b)**

of the total heat at the first core minimised the phase angle in the loop and in turn the acoustic losses.

The variation in acoustic power throughout the thermoacoustic loop using different heat ratios is given in Fig. **11**. It shows that the acoustic power flow is at the lowest level when using two-thirds of the total heat in the first stage, and the acoustic loop power increases gradually when increasing the heat ratio in the second core and reducing the ratio in the first heater. This is because the intensity of the acoustic oscillation in 60%:40% is not as strong as those in the other three heat ratio sets, as presented in Fig. **6** and **7**. For all the ratios, the curves again have the same relative characteristics. In the base case where the total heating power is split evenly between the two heaters, DeltaEC predicted that 58.4 W of the acoustic power from the resonance tube travels toward HHX2. Only 1 W is dissipated within AHX2. The remaining

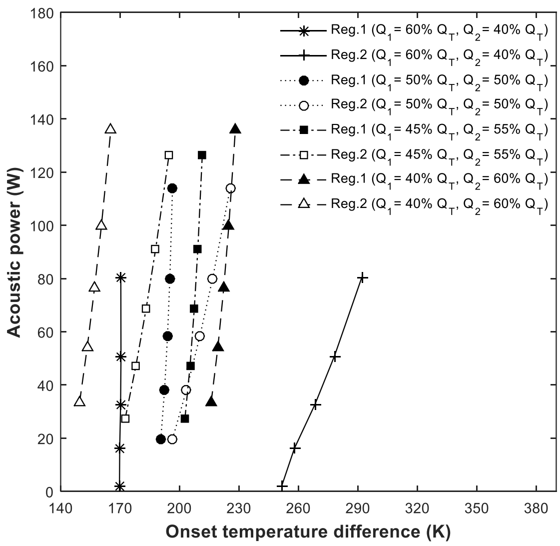

Fig. 12: Loop acoustic power relation with the temperature difference across the regenerator when the total heating power varies in the range of 2100 to 3000 W for three heat input ratios. Reg.1 represents regenerator of stage 1 (number 3 in Fig. **1(b)**), and Reg.2 represents regenerator of stage 2 (number 1 in Fig. **1(b)**).

57.4 W enters the cold side of regenerator 2 where the acoustic power is amplified to 77.5 W by consuming 1.25 kW of total thermal power. Minor losses of 1.8 W are incurred in HHX2, TBT2, and SAHX2. 24.4 W electrical power was extracted by the alternator (loudspeaker) with a thermal-to-acoustic conversion efficiency of 2.3%, an acoustic-to-electric efficiency of 41.8%, and a thermal-to-electric efficiency of 0.98%.

The onset temperature is also important to evaluate the performance of the thermoacoustic systems. The efficiency is generally better when the onset temperature is low. Therefore, to assess the current rig for the tested heat input percentages, the loop acoustic power is plotted against the temperature difference across the two regenerators in Fig. **12**. Clearly, the acoustic power amplification in the second regenerator decreases when the heat ratio into the first core is larger and the onset temperature increases in this case. However, in the first regenerator, the reverse happens. In fact, there is a significant drop in the onset temperature of the second core. This drop is larger in magnitude than the increase in the onset temperature of the first core. Generally, the onset temperature difference and the steepness of the loop power against temperature difference curve are indicators of the performance of a thermoacoustic system. A low onset temperature difference means low dissipation and adequate acoustic matching between the various components of the system. A steep power increase against temperature indicates good heat transfer of the AHXs and HHXs and also reflects low acoustic loss [31].

5. Validation of DeltaEC results

The results of the numerical modelling were surprising. More power is shown to be gained from the asymmetrical power distribution. Therefore, the performance of the experimental rig was assessed using the same operational concept. Fig. **13(a)** and **13(b)** compare the lab results of the same ratio of heating power (for total heat inputs of 2.1-3 kW), with the same load resistance of the alternator (loudspeaker) used in the DeltaEC simulation. Both the acoustic power and the electric output increase linearly with the total heat input. Extra power could be

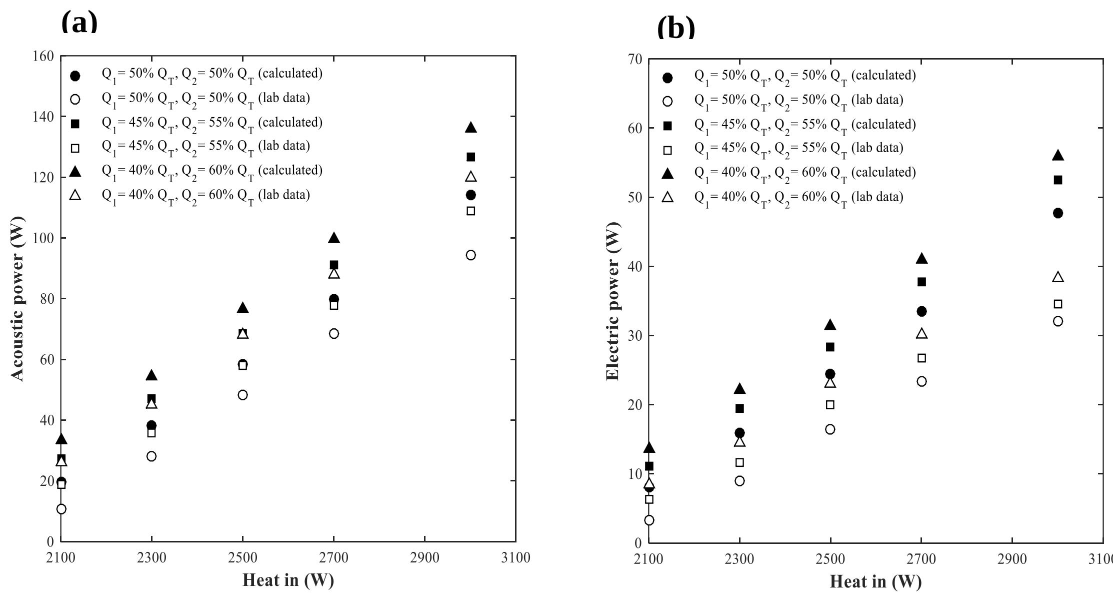

Fig. 13: Performance of the engine under four heat input ratios when the total heating power varies in the range of 2100 to 3000 W for three heat input ratios. **(a)** Acoustic power **(b)** Electrical power. Uncertainty is not significant so error bars are not included.

gained from the system by simply supplying a higher heat ratio into the second core. This is due to the stronger acoustic wave entering the alternator (loudspeaker) that is placed immediately after the second engine. The experimental data showed that with 2.5 kW total

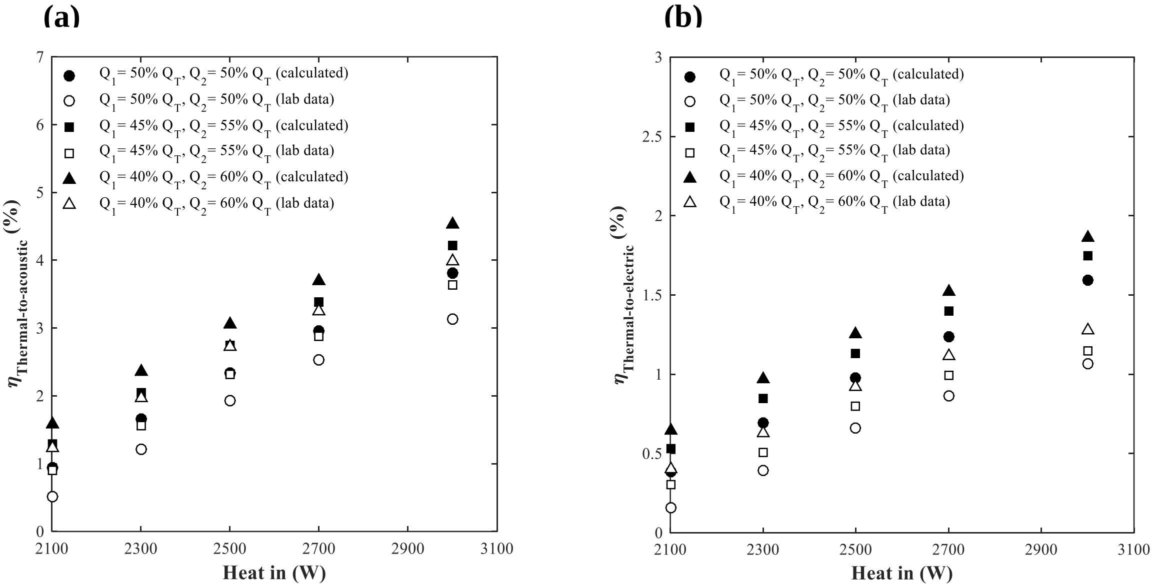

Fig. 14: Effect of the heating ratio on **(a)** thermal-to-acoustic efficiency and **(b)** thermal-to-electric efficiency for several heating powers when the total heating power varies in the range of 2100 to 3000 W for three heat input ratios. Uncertainty is not significant, so error bars are not included.

power added into the system with equal distribution across the two engines, the generated acoustic power is 48.4 W. This power is raised by approximately 41% to be 68 W when applying 40%:60%, and the electrical power is also increased from 16.5 to 23 W.

This implies that if a higher output power is required from the current design, one should apply lower heat power into core 1 and higher into core 2.

DeltaEC predictions are close to the measured values for all the heat input ratios at low power levels, while there is an overestimation in the numerical outputs at high input levels. This could be because the heat dissipations to the ambient are considerably higher at a higher heat input. Furthermore, the simulation predicted loop acoustic power values that were of the order of 11-17% larger than the lab ones, and electrical power values of the order of 27-32%. This suggests that the model does not account for all losses in converting thermal power into acoustic power, and that the heat dissipation is potentially an issue. For example, a considerable amount of the heat was being lost to the feedback pipe walls and at the top of the engine housing instead of being directed down into the working gas, which was not considered by DeltaEC. Also, the discrepancies in the electrical power reflect that the real loudspeaker is less efficient than the simulated version. Fig. **14(a)** and **14(b)** compare the DeltaEC model against the experimental values for the conversion efficiencies of the system for the four above-mentioned heat input percentages. The experimental results yielded a maximum value of the thermal-to-acoustic efficiency of 2.7% when using one-third and two-thirds of the total heat in the first and second heaters, respectively. At the same ratio, the thermal-to-electric efficiency reached a maximum value of 1.3%, which is lower than that noted in [68], where the LA acted as a transduction mechanism as well as a mechanical resonator.

The maximum error of the measured pressure amplitude, temperature, and electrical power output are $\pm 1.004\ Pa$, $\pm 1.095\ K$, and $\pm 0.118\ W$, respectively, and calculated based on the combined error from both systematic and random errors. The error of the thermal-to-acoustic efficiency and thermal-to-electric efficiency are ± 0.004, and ± 0.008, respectively.

In our current design, two main reasons contribute to the poorer efficiencies for the experimental data. The first reason is the higher parasitic losses through the engine casing, which can be reduced by having hot heat exchangers with staggered fins which will increase the heat transfer area, and therefore, significantly enhance the heat transfer rate. Furthermore, the working parcels inside the thermal buffer tube should ideally operate as a piston, transmitting only pressure and velocity oscillations from one side to the other. The gas should prevent heat leaks at the ends of the thermal buffer tube from each other. Convection within the thermal buffer tube is an issue because it can transfer enthalpy from one end to the other consuming heat from the hot heat exchanger.

The second reason is that the transduction efficiency of the loudspeaker is lower than the theoretical value (around 34%), which degraded the acoustoelectric conversion. It is possible that the measured electric output could be doubled by using the alternator reported in [50], which was approximately 60% efficient, or installing a bi-directional turbine. However, both are too expensive compared to the loudspeaker used in the double-core system, and this counteracts the affordability of the system for rural communities. Moreover, the alternator (loudspeaker) in this system is placed next to SAHX2. At this location, the acoustic impedance has a minimum value. In fact, the maximum alternator (loudspeaker) stroke is reached at 3 kW thermal power. Therefore, if more electrical power is to be extracted, and to avoid the stroke limitation, the driver should be installed in a high impedance zone.

Fig. **15** shows the acoustic power and the electric power as functions of the heat input ratio calculated using DeltaEC. The horizontal axis displays the ratio of the heat supply into the second core divided by the total heat added into the system. The predicted acoustic power increases gradually when the heat input power into the first engine is decreased and the heat input power into the second engine is increased until it reaches the highest level of 84 W at 30%:70%. The acoustic power declines when the heat input ratio is greater than 70% in HHX2. This behavior is mimicked by the electrical power output where the optimal is 34 W at 70% heat ratio in the second stage. Unfortunately, it was impossible to validate with the present experimental prototype due to material considerations of the HHXs, which is why the experimental results are restricted to a maximum ratio of 40%:60%.

At this point, the function of the regenerator and its relation to the power amplification and the heat input ratio can be discussed further.

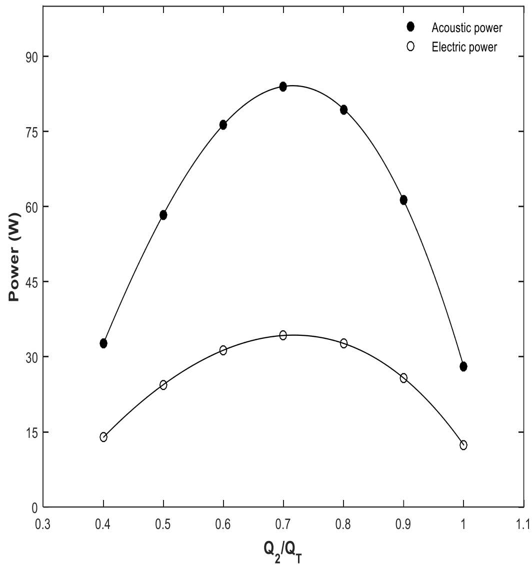

Fig. 15: Dependences of the acoustic power, the electric power as functions of the heating power percentage when the total heating power added into the system is 2500 W.

In a travelling-wave TAE, the regenerator acts as acoustic amplifier with the amplification factor, τ, given as the ratio of the hot-side temperature, T_H, to cold-side temperature, T_C:

$$\tau = \frac{T_H}{T_C} \tag{5}$$

The acoustic power flows out the regenerator can be expressed as:

$$P_{Ac.,out} = \tau P_{Ac.,in} \tag{6}$$

Where $P_{Ac.,in}$ and $P_{Ac.,out}$ are respectively the acoustic power flows into the ambient end and out of the hot end of the regenerator. Therefore, the regenerator produces a net acoustic power as follows [28]:

$$P_{Ac.,net} = (\tau - 1) P_{Ac.,in} \tag{7}$$

The acoustic power flows into the ambient end of the regenerator can be expressed as a function of the pressure amplitude as:

$$P_{Ac.,in} = \frac{A_g |p_{1,in}|^2}{2Re[n\rho_m a]} \tag{8}$$

Here: $|p_{1,in}|$ is the pressure amplitude at the ambient end of the regenerator, A_g is the area of the regenerator, ρ_m the mean density of the working gas, a the speed of sound, and n is the ratio of the acoustic impedance to the specific acoustic impedance for the regenerator. This ratio (also called the impedance enhancement) is set by the system configuration (bypass, or looped tube) [31]. Substituting Eq.(8) with Eq.(7) gives the net acoustic power produced by the regenerator in the form:

$$P_{Ac.,net} = (\tau - 1) \frac{A_g |p_{1,in}|^2}{2Re[n\rho_m a]} \tag{9}$$

Table 3. Summary of DeltaEC results of the engine using different heat input ratios

Parameter	Heat input percentage, Q_1/Q_T 0.6	0.5	0.4
Total heat input, Q_T (kW)	2.5	2.5	2.5
Pressure at cold end of regenerator 1, $\lvert p_1 \rvert$ (Pa)	2745	3525	3849
Pressure at cold end of regenerator 2, $\lvert p_1 \rvert$ (Pa)	1939	2782	3431
Volumetric velocity at cold end of regenerator 1, $\lvert U_1 \rvert$ (m^3/**s)**	0.017	0.027	0.035
Volumetric velocity at cold end of regenerator 2, $\lvert U_1 \rvert$ (m^3/**s)**	0.034	0.042	0.045
Cold temperature of reg.1, T_C (K)	369	371	373
Hot temperature of reg.1, T_H (K)	637	581	530
Cold temperature of reg. 2, T_C (K)	363	363	363
Hot temperature of reg. 2, T_H (K)	533	557	585
Amplification factor at reg.1, τ	1.73	1.57	1.42
Amplification factor at reg.2, τ	1.47	1.53	1.61
Impedance enhancement at reg.1, n	17.2	14.4	11.9
Impedance enhancement at reg.2, n	6.2	7.2	8.3
Net acoustic power produced by reg.1, $P_{Ac., net}$ (W)	17.2	26.9	29.0
Net acoustic power produced by reg.2, $P_{Ac., net}$ (W)	15.1	31.5	47.4
Thermal-to-acoustic efficiency, (%)	1.3	2.3	3.1
Thermal-to-electrical efficiency, (%)	0.6	1.0	1.3

Eq.(9) shows that the net acoustic power is a function of the square of the pressure amplitude at the cold side of the regenerator, the amplification factor and the acoustic impedance enhancement. Table.**3** is provided to illustrate the behavior of the two regenerators with the novel operational methodology applied in this study.

The numerical data shows that when the heat input ratio is varied from 0.6 to 0.4, the pressure amplitude, $|p_1|$, at the cold end of regenerator 1 and regenerator 2 increases significantly. Thus, a strong acoustic wave is produced which is clearly seen in Fig. **5**. Also, the volumetric velocity, $|U_1|$, increases in both the regenerators. The thermal dissipation is proportional to $\left|p_{1,in}\right|^2$, and the viscous dissipation is proportional to $\left|U_{1,in}\right|^2$, which reflects that the losses become larger with higher heating percentages. The calculated thermal and viscous losses in the two regenerators are less than 1 W in all the tested heat ratios, which means they have no significant effect.

According to Eq.(9), the net production of the acoustic power is proportional to the square of the pressure amplitude, the amplification factor, and the inverse of the impedance enhancement. As appeared in Table 3, the net produced acoustic power from the two regenerators for the 0.6 heat input ratio in the second engine is significantly increased due to the significant increase in the pressure amplitude in the two regenerators; $|p_1|$ is increased from 2745 to 3949 Pa in regenerator 1, and from 1939 to 3431 in regenerator 2, when the heat ratio is changed from 0.4 to 0.6. As a result, the net acoustic power from regenerator 1 changed from 17.2 to 29 W in regenerator 1, and from 15.1 to 47 W in regenerator 2. Moreover, due to the heat input methodology, the impedance enhancement in both regenerators tends toward 10-20, which is close to the preferred conditions to reduce viscous losses in travelling-wave systems [31].

To be clear, the TAE had previously been optimised for even heat input [67]. At 50%:50%, the TAE generated 16.5 W. With no change in configuration, the output power increased to 23 W electrical power when the heat distributed ratio was adjusted to 40% in the first engine stage and 60% in the second one. This is around a 39% increase in the electricity with no additional changes to the system other than the distribution of heat flow. As discussed in the introduction, there are many variations of TAEs and many of them are multicore with a single power extraction. One drive to publish these results is the desire to see if this increase can be achieved with other designs, or if it is only valid for the SCORE design.

For this reason, it is interesting to note that [69] identified that the symmetrical geometry conditions led to an asymmetrical acoustic condition in their three-stage travelling-wave TAE. Although their three engine stages have exactly symmetric configuration, the produced acoustic power and thermodynamic efficiencies are different for each engine stage. This suggests that the phenomena might also be present in other multistage systems and that these designers might want to consider whether asymmetric heat input might increase their electrical output.

6. Summary and Conclusions

In this work, a TAE is used to convert thermal energy into acoustic power and then into electricity with air at atmospheric pressure as the working gas. A looped-tube TAE with two heat sources is considered. A numerical model of the looped-tube double-core TAE has been developed with the simulation software DeltaEC, which is validated later through experimental tests. Particular emphasis has been placed on investigating the effect of heat input distribution from such a double heat source on the conversion of acoustic power. The effect of different heat source on heat-to-acoustic energy conversion is investigated. The total heating power in the two-core system is varied to be asymmetrical. The two heater blocks are set to deliver asymmetric thermal energies.

The pressure amplitude, volumetric velocity amplitude, their phases, the acoustic impedance, and the onset temperature difference have been examined. The results shown that the tested parameters are significantly influenced by the way of inputting the thermal energy from the heat distribution sources, and as a result, both the acoustic and electrical power outputs increase. The physical process of the amplification sound wave in the regenerators by inputting different thermal energies from the multiple heat sources is mathematically illustrated and analysed. When the heating power is higher in the first engine core, nonlinearity affects the power conversion. On the other hand, when the input power from the first heater is lower, thermoacoustic oscillations are shown to be amplified.

The power output obtained from the numerical model was shown to be greatest at heat ratio 30%:70%. However, using this ratio in the experimental tests was not possible due to the strength limitation of the material of the HHX.
The simulated loop acoustic power increased to 68.6 W when 40%:60% heat input is applied with no other changes to configuration. For the same ratio, the electrical power increased from 24.4 W to 31.4 W. A similar 39% increase of electrical output was observed in the experimental results, showing that this is not an artifact of the DeltaEC program. Compared to SCORE project tests of the same experimental apparatus, the current work improved the electrical output by 149%. We suggest other researchers using a multistage system look to determine if this is a general design tip or just specific to certain types of multistage design. However, results suggesting that this occurs elsewhere can be found in the literature.
This new heat input strategy makes it possible to meet the 50 – 100 W target identified as a requirement if this technology is to be implemented in the field, if further modification with a known effect, such as pressurisation to 4 bar were to be implemented. Further research is needed to see if this improved strategy can be integrated into a new, more compact design that still meets the cost requirements.

7. Acknowledgements

The authors would like to acknowledge the support for this research received from the University of Nottingham and The Gordon Memorial College Trust Fund GMCTF. The SCORE project was funded by the EPSRC (grant EP/E044379) and was a research partnership that brought together the University of Nottingham, City University London, Leicester University, Queen Mary University of London and Practical Action.

8. References

[1] Sanchez T, Dennis R, Pullen KR. Cooking and lighting habits in rural Nepal and Uganda. Proc Inst Mech Eng Part A J Power Energy 2013. https://doi.org/10.1177/0957650913498872.

[2] Kanagawa M, Nakata T. Assessment of access to electricity and the socio-economic impacts in rural areas of developing countries. Energy Policy 2008. https://doi.org/10.1016/j.enpol.2008.01.041.

[3] Bhattacharyya SC, Bhattacharyya SC. Energy Access. Energy Econ., 2019. https://doi.org/10.1007/978-1-4471-7468-4_17.

[4] Sanchez, T., Owala, H. and Okello V. Research into the behaviour of rural families to technology changes. Proc. Int. Conf. low-cost, Electr. Gener. heat engines Rural areas., n.d.

[5] Riley PH. Affordability for sustainable energy development products. Appl Energy 2014;132:308–16. https://doi.org/10.1016/j.apenergy.2014.06.050.

[6] Riley PH, Saha CR, Johnson CM. Designing a low-cost, electricity-generating cooking stove. IEEE Technol Soc Mag 2010;29:47–53. https://doi.org/10.1109/MTS.2010.937029.

[7] Ramos A, Chatzopoulou MA, Freeman J, Markides CN. Optimisation of a high-efficiency solar-driven organic Rankine cycle for applications in the built environment. Appl Energy 2018. https://doi.org/10.1016/j.apenergy.2018.06.059.

[8] Rahbar K, Mahmoud S, Al-Dadah RK, Moazami N, Mirhadizadeh SA. Review of organic Rankine cycle for small-scale applications. Energy Convers Manag 2017. https://doi.org/10.1016/j.enconman.2016.12.023.

[9] Li G. Organic Rankine cycle environmental impact investigation under various working fluids and heat domains concerning refrigerant leakage rates. Int J Environ Sci Technol 2019. https://doi.org/10.1007/s13762-018-1686-y.

[10] Hsu CT, Huang GY, Chu HS, Yu B, Yao DJ. Experiments and simulations on low-temperature waste heat harvesting system by thermoelectric power generators. Appl Energy 2011. https://doi.org/10.1016/j.apenergy.2010.10.005.

[11] Elghool A, Basrawi F, Ibrahim TK, Habib K, Ibrahim H, Idris DMND. A review on heat sink for thermo-electric power generation: Classifications and parameters affecting performance. Energy Convers Manag 2017. https://doi.org/10.1016/j.enconman.2016.12.046.

[12] Gou X, Yang S, Xiao H, Ou Q. A dynamic model for thermoelectric generator applied in waste heat recovery. Energy 2013. https://doi.org/10.1016/j.energy.2013.01.040.

[13] Chen M, Lund H, Rosendahl LA, Condra TJ. Energy efficiency analysis and impact evaluation of the application of thermoelectric power cycle to today's CHP systems. Appl Energy 2010. https://doi.org/10.1016/j.apenergy.2009.06.009.

[14] Riley PH. The Myth of the High-Efficiency External-Combustion Stirling Engine. Engineering 2015;07:789–95. https://doi.org/10.4236/eng.2015.712068.

[15] Muralidharan V, Sussan TE, Limaye S, Koehler K, Williams DL, Rule AM, et al. Field testing of alternative cookstove performance in a rural setting of Western India. Int J Environ Res Public Health 2015. https://doi.org/10.3390/ijerph120201773.

[16] Mechanics PS-J of AF, 2011 undefined. Hot Air Engines. SearchEbscohostCom n.d.

[17] Kautz M, Hansen U. The externally-fired gas-turbine (EFGT-Cycle) for decentralized use of biomass. Appl Energy 2007;84:795–805. https://doi.org/10.1016/j.apenergy.2007.01.010.

[18] Zanzig J. The stirling cycle engine. SAE Tech. Pap., 1963. https://doi.org/10.4271/630315.

[19] Wan Dawi SMH, Othman MM, Musirin I, Kamaruzaman AAM, Arriffin AM, Salim NA. Gamma Stirling engine for a small design of renewable resource model. Indones J Electr Eng Comput Sci 2017. https://doi.org/10.11591/ijeecs.v8.i2.pp350-359.

[20] YOSHIHARA S, HOSHINO T. Model free piston Stirling engine. Proc Symp Stirlling Cycle 2003. https://doi.org/10.1299/jsmessc.2003.7.87.

[21] Rott N. Damped and thermally driven acoustic oscillations in wide and narrow tubes. Zeitschrift Für Angew Math Und Phys ZAMP 1969. https://doi.org/10.1007/BF01595562.

[22] Ceperley PH. A pistonless Stirling engine—The traveling wave heat engine. J Acoust Soc Am 1979. https://doi.org/10.1121/1.383505.

[23] Ward WC, Swift GW. Design environment for low-amplitude thermoacoustic engines. J Acoust Soc Am 1994. https://doi.org/10.1121/1.409938.

[24] Swift GW. Analysis and performance of a large thermoacoustic engine. J Acoust Soc Am 1992. https://doi.org/10.1121/1.403896.

[25] Backhaus S, Swift G. New Varieties of Thermoacoustic Engines. Ninth Int Congr Sound Vib 2002.

[26] Swift GW. Thermoacoustic engines. J Acoust Soc Am 1988;84:1145–80.

[27] Piccolo A. Design issues and performance analysis of a two-stage standing wave thermoacoustic electricity generator. Sustain Energy Technol Assessments 2018;26:17–27.

[28] Backhaus S, Swift GW. A thermoacoustic-Stirling heat engine: Detailed study. J Acoust Soc Am 2000;107:3148–66.

[29] Backhaus S, Swift GW. A thermoacoustic Stirling heat engine. Nature 1999;399:335.

[30] Tijani MEH, Spoelstra S. A high performance thermoacoustic engine. J Appl Phys 2011;110:1145. https://doi.org/10.1063/1.3658872.

[31] De Blok K. Low operating temperature integral thermo acoustic devices for solar cooling and waste heat recovery. J Acoust Soc Am 2008;123:3541.

[32] Abdoulla-Latiwish KOA, Mao X, Jaworski AJ. Thermoacoustic micro-electricity generator for rural dwellings in developing countries driven by waste heat from cooking activities. Energy 2017. https://doi.org/10.1016/j.energy.2017.05.029.

[33] Wang K, Sun D, Zhang J, Xu Y, Zou J, Wu K, et al. Operating characteristics and performance improvements of a 500 W traveling-wave thermoacoustic electric generator. Appl Energy 2015;160:853–62.

[34] Badi AP, Beheshti H. Numerical Study of Multistage Serial and Parallel Configurations of Thermoacoustic Engines. J Therm Sci Eng Appl 2016;8:21025.

[35] Kang H, Cheng P, Yu Z, Zheng H. A two-stage traveling-wave thermoacoustic electric generator with loudspeakers as alternators. Appl Energy 2015;137:9–17. https://doi.org/10.1016/j.apenergy.2014.09.090.

[36] Wu Z, Yu G, Zhang L, Dai W, Luo E. Development of a 3 kW double-acting thermoacoustic Stirling electric generator. Appl Energy 2014;136:866–72.

[37] Wang K, Qiu L. Numerical analysis on a four-stage looped thermoacoustic Stirling power generator for low temperature waste heat. Energy Convers Manag 2017;150:830–7.

[38] K DeBlok. 10kW bi-directional turbine n.d.

[39] Dennis R, Pullen K. Development of a wood-fired cooking stove to incorporate a thermo-acoustic engine-generator unit. Proc Inst Mech Eng Part A J Power Energy 2013;227:740–51.

[40] Okello V, Owala H, Sanchez T. The reaction of rural families in Kenya to technology changes. Proc Inst Mech Eng Part A J Power Energy 2013;227:752–61.

[41] Hutton G, Rehfuess E, Tediosi F. Evaluation of the costs and benefits of interventions to reduce indoor air pollution. Energy Sustain Dev 2007;11:34–43.

[42] Bates L, Theuri D, Owala H, Okello V, Hada J, Bikram Malla M, et al. Smoke, health

and household energy. Participatory methods for design, installation, monitoring and assessment of smoke alleviation technologies. Smoke, Heal. Househ. energy. Particip. methods Des. Install. Monit. Assess. smoke alleviation Technol., DFID; 2005.

[43] Shahsavari A, Akbari M. Potential of solar energy in developing countries for reducing energy-related emissions. Renew Sustain Energy Rev 2018;90:275–91.

[44] Kabir E, Kumar P, Kumar S, Adelodun AA, Kim K-H. Solar energy: Potential and future prospects. Renew Sustain Energy Rev 2018;82:894–900.

[45] Saechan P, Jaworski AJ. Thermoacoustic cooler to meet medical storage needs of rural communities in developing countries. Therm Sci Eng Prog 2018.

[46] Xu J, Zhang L, Hu J, Wu Z, Bi T, Dai W, et al. An efficient looped multiple-stage thermoacoustically-driven cryocooler for liquefaction and recondensation of natural gas. Energy 2016;101:427–33.

[47] Garrett SL, Smith JA, Smith RWM, Heidrich BJ, Heibel MD. Fission-powered in-core thermoacoustic sensor. Appl Phys Lett 2016;108:144102.

[48] Ali RA, Garrett SL, Smith JA, Kotter DK. Thermoacoustic thermometry for nuclear reactor monitoring. IEEE Instrum Meas Mag 2013;16:18–25.

[49] Swift GW. Thermoacoustics: A unifying perspective for some engines and refrigerators. Springer; 2017.

[50] Saha CR, Riley PH, Paul J, Yu Z, Jaworski AJ, Johnson CM. Halbach array linear alternator for thermo-acoustic engine. Sensors Actuators, A Phys 2012;178:179–87. https://doi.org/10.1016/j.sna.2012.01.042.

[51] De Blok CM, Owczarek P, Francois M. Bi-directional turbines for converting acoustic wave power into electricity. 9th PAMIR Int. Conf., 2014.

[52] Tourkov K, Schaefer L. Effect of regenerator positioning on thermoacoustic effect in a looped tube traveling wave thermoacoustic engine. Energy Convers Manag 2015;95:94–100.

[53] Kruse A, Ruziewicz A, Tajmar M, Gnutek Z. A numerical study of a looped-tube thermoacoustic engine with a single-stage for utilization of low-grade heat. Energy Convers Manag 2017;149:206–18.

[54] Jin T, Yang R, Wang Y, Liu Y, Feng Y. Phase adjustment analysis and performance of a looped thermoacoustic prime mover with compliance/resistance tube. Appl Energy 2016;183:290–8.

[55] Sun DM, Wang K, Zhang XJ, Guo YN, Xu Y, Qiu LM. A traveling-wave thermoacoustic electric generator with a variable electric R-C load. Appl Energy 2013;106:377–82. https://doi.org/10.1016/j.apenergy.2013.01.051.

[56] Yu Z, Jaworski AJ, Backhaus S. Travelling-wave thermoacoustic electricity generator using an ultra-compliant alternator for utilization of low-grade thermal energy. Appl Energy 2012;99:135–45. https://doi.org/10.1016/j.apenergy.2012.04.046.

[57] Yu Z, Jaworski AJ, Backhaus S. A low-cost electricity generator for rural areas using a travelling-wave looped-tube thermoacoustic engine. Proc Inst Mech Eng Part A J Power Energy 2010;224:787–95.

[58] Chen BM, Riley PH, Abakr YA, Pullen K, Hann DB, Johnson CM. Design and development of a low-cost, electricity-generating cooking Score-Stove^{TM}. Proc Inst Mech Eng Part A J Power Energy 2013;227:803–13. https://doi.org/10.1177/0957650913498733.

[59] Ehsan M, Sarker M, Mahmud R, Riley PH. Performance of an electricity-generating cooking stove with pressurized kerosene burner. Procedia Eng., vol. 105, 2015, p. 619–27. https://doi.org/10.1016/j.proeng.2015.05.040.

[60] Chen BM, Abakr YA, Riley PH, Hann DB. Development of thermoacoustic engine operating by waste heat from cooking stove. AIP Conf. Proc., vol. 1440, 2012, p. 532–40. https://doi.org/10.1063/1.4704259.

[61] Ward WC, Swift GW. Design environment for low-amplitude thermoacoustic engines. J Acoust Soc Am 1994;95:3671–2.

[62] Ward B, Clark J, Swift GW. Design environment for low-amplitude thermoacoustic energy conversion, DeltaEC Version 6.4 b2 Users Guide. Los Alamos Natl Lab Netw 2016.

[63] Timmer MAG, de Blok K, van der Meer TH. Review on the conversion of thermoacoustic power into electricity. J Acoust Soc Am 2018;143:841–57.

[64] de Blok K. Novel 4-stage traveling wave thermoacoustic power generator. ASME 2010 3rd Jt. US-European fluids Eng. summer Meet. collocated with 8th Int. Conf. nanochannels, microchannels, minichannels, American Society of Mechanical Engineers Digital Collection; 2011, p. 73–9.

[65] Fusco AM, Ward WC, Swift GW. Two-sensor power measurements in lossy ducts. J Acoust Soc Am 1992;91:2229–35.

[66] De Blok K. Acoustic power measurements in thermoacoustic systems. 2013.

[67] Riley PH. Designing a low-cost electricity-generating cooking stove for high-volume implementation. University of Nottingham, 2014.

[68] Backhaus S, Tward E, Petach M. Traveling-wave thermoacoustic electric generator. Appl Phys Lett 2004;85:1085–7.

[69] Yu Z, Al-Kayiem A. Numerical analysis of a thermally driven thermoacoustic heat pump for low-grade heat recovery. Comput Therm Sci An Int J 2014;6.